Eur. Phys. J. Special Topics **223**, 2269–2283 (2014)

DOI: 10.1140/epjst/e2014-02263-2

THE EUROPEAN PHYSICAL JOURNAL SPECIAL TOPICS

Review

Morphodynamic modeling of aeolian dunes: Review and future plans

E.J.R. Parteli[1,a], K. Kroy[2,b], H. Tsoar[3,c], J.S. Andrade Jr.[4,d], and T. Pöschel[1,e]

[1] Institut für Multiskalensimulation, Friedrich-Alexander-Universität Erlangen-Nürnberg, 91052 Erlangen, Germany
[2] Institut für Theoretische Physik, Universität Leipzig, Postfach 100920, Leipzig 04009, Germany
[3] Department of Geography and Environmental Development, Ben-Gurion University of the Negev, Beer Sheva 84105, Israel
[4] Departamento de Física, Universidade Federal do Ceará, 60455-760, Fortaleza, Ceará, Brazil

Received 6 May 2014 / Received in final form 18 August 2014
Published online 24 October 2014

Abstract. Sand dunes are ubiquitous in deserts, on coasts, on the sea bottom, and on the surface of Mars, Venus and Titan. The quantitative understanding of dune dynamics is thus of relevance for a broad range of physical, geological and planetary sciences. A morphodynamic model for dunes, which combines an analytical description of the average turbulent wind field over the topography with a continuum saltation model, has proven successful to quantitatively reproduce the shape of aeolian dunes of different types. We present a short review on the physics of dune formation and the model development, as well as some future plans for further developments and applications.

1 Introduction

Dunes form wherever a sediment bed is exposed to a medium (such as air or water) that entrains particles into surface flow. The primary mechanism of surface transport leading to aeolian dunes is *saltation*, which consists of particles moving close to the surface in nearly ballistic trajectories, thereby ejecting new particles upon collision with the sediment bed [1]. To understand dunes, one first has to understand this grain hopping excited by strong winds. The aim is then to predict the rich variety of dune shapes occurring in Nature (see Fig. 1) from a mathematical model of the saltation process.

[a] e-mail: eric.parteli@fau.de
[b] e-mail: klaus.kroy@uni-leipzig.de
[c] e-mail: tsoar@bgu.ac.il
[d] e-mail: soares@fisica.ufc.br
[e] e-mail: thorsten.poeschel@fau.de

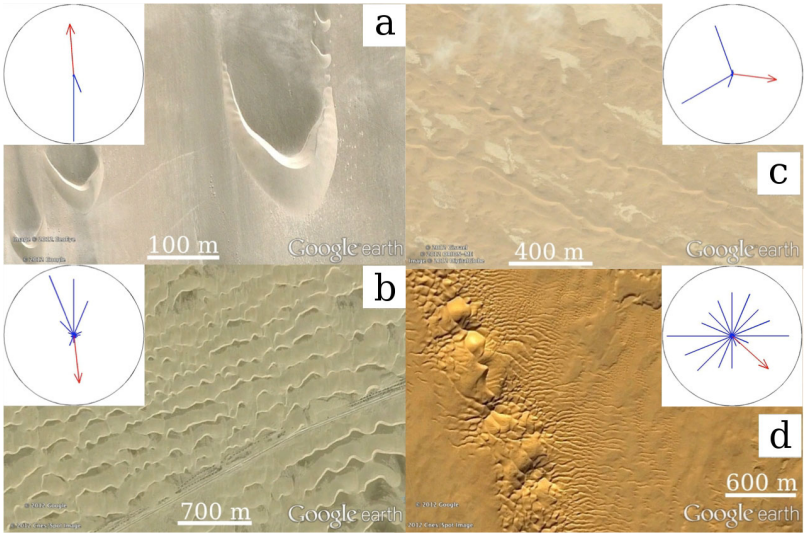

Fig. 1. Images of the four main types of dunes together with the respective sand roses. In all images, north is at top. The dunes are near 15°07S, 75°15W (a); 25°49N, 49°55E (b); 30°52N, 33°52E (c), and 30°35N, 2°51E (d) (images credit: Google Earth). A sand rose represents the potential sand drift from the 16 directions of the compass (see Ref. [2]). The arms of the sand rose are proportional in length to the drift potential DP_i, that is the potential rate of sand transport due to winds above threshold [2–4] *from* a given direction i, while the red arrow in the sand rose indicates the resultant sand transport trend. The total drift potential is given by $\mathrm{DP} = \sum_i \mathrm{DP}_i$, while the so-called resultant drift potential is given by the equation $\mathrm{RDP} = |\sum_i \mathrm{DP}_i \mathbf{e}_i|$, where $\mathbf{e}_i$ is the unit vector pointing in the direction i. Barchans (a) and transverse dunes (b) are *migrating* dunes, which form under nearly unidirectional flows (see Fig. 2) or $r \equiv \mathrm{RDP}/\mathrm{DP} \gtrsim 0.8$. In contrast, longitudinal seif dunes (c) are *elongating* dunes, which form when the flow has two main directions with obtuse divergence angle and $r \lesssim 0.6$ [5,6] (see Figs. 3h and 6b). Indeed, most active sand dunes of the world are under both mechanisms of migration and elongation since in most cases sand roses display several wind directions of different transport rates and r is typically within the range $0.1 < r < 0.8$. The associated "hybrid" dune shapes (also called *oblique* dunes) can be either similar to barchans and transverse dunes when $r > 0.7$ or to seif dunes when $r < 0.7$ (see Figs. 3f,g and Refs. [5,7,8]). At very low r ($\lesssim 0.4$), that is under flow regimes with high directional variability, dunes are of *accumulating* type, of which the star dune (d) is the representative example [9,10]. While the minimal size of dunes is set by the flux saturation length (see text), their maximal size is bound by the thickness of the atmospheric boundary layer as shown in Ref. [11].

This natural process, which is familiar to everybody who has spent a windy day at a sandy beach, not only creates the various types of dunes illustrated in the figure, but also ordered sand structures on much smaller (ripples) and larger (megadunes, dune fields) scales. The observer of this rich phenomenology "never fails to be amazed at a simplicity of form, an exactitude of repetition and geometric order unknown in nature on a scale larger than that of crystalline structure" [1]. The strong discrepancy between the apparent disorder on the grain scale and the striking regularities and similarities exhibited by the emerging structures clearly calls for a generic physical explanation. It makes one suspect a robust basic mechanism, hidden beneath the virtually infinite possible variations imposed by variable weather and boundary conditions, from which the most salient qualitative features underlying this prolific structure formation should become understandable.

Attempts to reveal this basic mechanism date back to Bagnold's seminal work in the mid 20th century [1]. The construction of a mathematical minimal model that clearly pinpoints the physical principles underlying dune formation was only achieved half a century later, though [12–14], as recapitulated in Sect. 2.1, below. We then summarize how the focus subsequently shifted towards applications addressing increasingly complex and less accessible (e.g. extraterrestrial) structures in Sect. 2.2. Our discussion mostly concentrates on dunes and barely touches on ripples. While the small beach ripples may superficially look simpler than the large dunes and sand seas, and much has been written about them, their physics turns out to be more complex. It crucially depends on mesoscale details of the grain hopping that are only of minor relevance for a qualitative understanding of dunes. In Sect. 3.1, we discuss recent attempts to get hold of the mesoscale physics by improved sediment transport models, which promise to open the way to a new aera of mesoscale modeling and applications (see Sect. 3.2), including the modeling of aeolian ripples and subaqueous bedforms.

2 Morphodynamic modeling: Review and state-of-the-art

2.1 Minimal model for dunes

A rational approach aiming at a qualitative understanding of dune formation and migration naturally tries to coarse-grain the complexity on the grain scale as much as possible and concentrates on the basic physics that determines its most salient features. The central quantity one needs to know is the overall sand flux as a function of the wind speed, sand supply and topography. Thanks to a strong scale separation between the grain trajectories and the dunes, the challenging task can essentially be divided into three subtasks. One firstly needs to know the stationary wind stress exerted onto a given sand topography; secondly, the resulting spatially resolved sand erosion and deposition causing its (slow) time evolution; finally, the feedback of the grain transport process onto the wind. All three aspects need first of all to be qualitatively understood for an isolated dune exposed to a unidirectional, uniform wind, quantitative details and environmental complications can be taken care of later [15,16].

As it turns out [13,14], there are two relatively small but crucial qualitative features that have to be retained in a minimal model for aeolian dunes: the spontaneous symmetry breaking of the turbulent wind over a smooth terrain [17,18]; and the emergence of a characteristic mesoscale for the retardation of the sand flux with respect to the wind (the so-called "*saturation length*" L_{sat}) [12]. These features are illustrated in Fig. 2a. The first effect renders a flat sand bed unstable and selects a finite windward dune slope [14,21], as required for autonomous structure formation. The second introduces a minimum dune size [13,14,21,22] and entails a non-trivial scaling of the topography (and its time evolution) with scale transformations and ambient conditions, governed by powerful shape attractors [23]. These predictions were corroborated by field measurements [24,25] (see also Ref. [26]) and by lab experiments with scaled-down subaqueous dunes [25,27–29]. In particular, the minimum dune, which actually is a very flat dome-shaped heap, is predicted to have a finite length proportional to L_{sat} [13,14,30–32]. Given sufficient influx, its slope and mass grows towards a limiting value that depends on wind and sand supply. Beyond a certain critical slope, a shape transition occurs. The dune ceases to be a smooth heap of sand, avalanches and flow separation give rise to the formation of a slip-face and a wake zone, on the lee side of the dune (Figs. 2b,c). The critical size for this shape transition is predicted to be strongly dependent on the influx saturation [23,31].

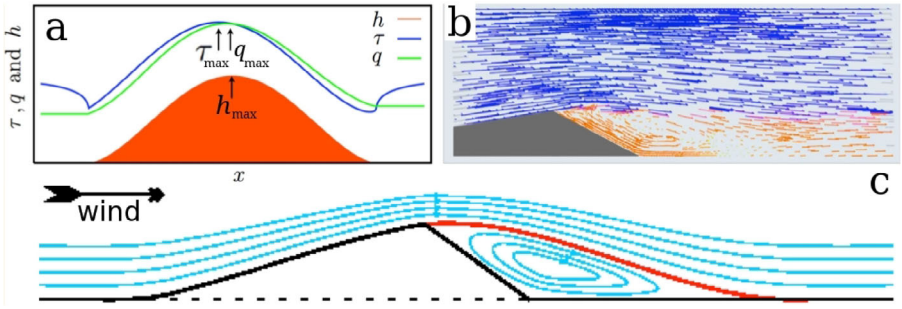

Fig. 2. (a) Sand flux over a dune profile $h(x)$ (aspect ratio not to scale for better visibility), which actually is a flat smooth heap of sand. Note that the wind shear stress $\tau(x)$ attains its maximum slightly upwind of the crest. Dune formation is due to this fundamental symmetry breaking. The actual flux $q(x)$ lags behind the nominal saturated flux $q_s(x) \propto \tau(x)$ due to saturation transients, which are responsible for the existence of a minimum dune size and the shape transition from a smooth dome-shaped heap of sand to a sawtooth-shaped dune with brink and slipface. In panel (b) we see an example of such a sharp-crested dune shape. This panel displays the wind velocity vectors, colored by velocity magnitude (increasing from red to blue), over the cut along the symmetry plane of a barchan (solid surface), obtained using Computational Fluid Dynamics (CFD) simulations [14]. The wind speed of the recirculating flow in the wake zone is usually subcritical, so that no sizable downwind sand transport occurs, there. (c) To make the analytical minimal model applicable to such cases, a phenomenological parametrization of the separation bubble between the brink and the bed is employed. The flow over the envelope covering the dune profile and the wake zone is smooth and remains accessible to the analytical theory [14,19]. In Ref. [15], the model is extended to the lateral component of the wind shear stress [18] to make it applicable for simulating three-dimensional dune shapes. In practice, this is done by iteratively performing the following steps: (i) first, the average turbulent wind shear stress profile over the envelope comprising the terrain and the separation bubble is computed using an analytical model [17,18,20], whereas the separation streamline is applied to each longitudinal slice (along the wind direction) of the three-dimensional dune shape; (ii) next, the height-integrated mass flux of saltating particles is calculated using the continuum saltation model of Ref. [12], whereupon (iii) the changes in local height are computed from mass conservation; (iv) wherever the local slope exceeds the angle of repose of the sand (34°), the surface instantaneously relaxes through avalanches in the direction of the steepest descent [13–16].

In subsequent years, insights gained from the minimal model have been used in diverse numerical approaches. Important examples include the skeleton model [33], which is a highly efficient intermediate model between the two-dimensional and full three-dimensional implementations of the minimal model; cellular automaton models, in which the surface evolution is dictated by probabilistic rules [34], and dune field models, where dunes are treated as "interacting particles" [35,36] (for reviews see Refs. [37,38]). Moreover, key elements of the minimal model have been scrutinized with great effort, theoretically and experimentally. Recent work has e.g. considered more closely the minimum dune size [39], the wind shear stress exerted by the air onto a dune [40] and the detailed behavior of the saturation length for subaqueous sand transport [40,41]. These studies have provided valuable additional insights but, by and large, confirmed the basic structure and predictions of the minimal model. We therefore do not dwell on these developments further, here, but rather turn to some recent extensions and applications aimed at gaining a better understanding of complex sand topographies on Earth and Mars.

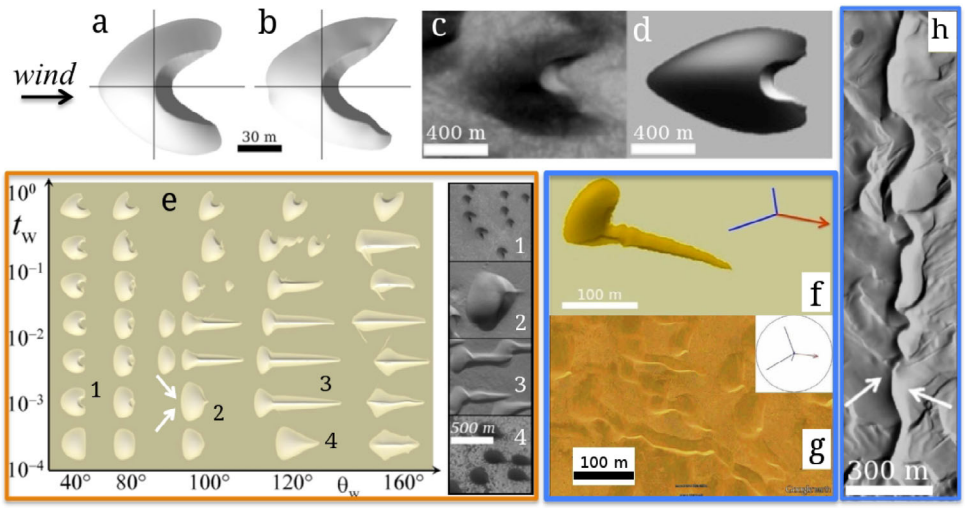

Fig. 3. (a) Simulation and (b) measured profile of a barchan in Morocco [48]; (c) simulation and (d) images of a barchan in Arkhangelsky crater, Mars [43]; (e) phase diagram of dune morphology obtained in simulations using bimodal winds with different divergence angles θ_w and non-dimensional rescaled durations ($t_w = T_w/T_m$), where T_m is the barchan turnover time, that is the time needed for the barchan to migrate a distance equal to its size [6]. Numbers indicate Martian dune shapes of the images on the right panel (images credit: NASA/JPL/MSSS); (f) simulation and (g) image of an asymmetric barchan in Sinai (north is at top; image credit: Google Earth) [8]; (h) simulation of a longitudinal seif dune on a sand bed (arrows indicate the wind directions of the bimodal wind) [6].

2.2 Model extensions and applications

Barchans – In Ref. [16] the model was applied to simulate the three-dimensional shape of a barchan in Morocco. Quantitative agreement was found between predicted and measured dune profiles (Figs. 3a,b). Also quantitative agreement was found between predicted and measured profiles of the wind velocity and sand flux over the longitudinal cut along the symmetry axis of a barchan in Brazil [42]. Using attributes of sediment and atmosphere for Mars, Ref. [43] reproduced the shape of barchans at Martian Arkhangelsky crater (Figs. 3c,d) and showed that the characteristic elongated shape – that is, the large along-wind to cross-wind width ratio – of Martian intra-crater dunes [44] may result from low values of the upwind shear stress relative to the threshold for sand transport [43].

Dunes under varying wind directions – To simulate a change in wind direction, the field is rotated by an angle θ_w (the divergence angle between both directions), while the wind direction is kept constant [5]. After rotation of the field, the dune's separation bubble adapts to the new wind direction. In Refs. [6,43], this model was applied to calculate dune formation under bimodal winds, where the wind oscillates between two directions of duration T_w. Transverse (longitudinal) dune alignment is obtained for acute (obtuse) θ_w (see Fig. 3e), in agreement with the theoretical prediction [5] that dune alignment is such that it leads to the maximal gross bedform-normal transport – defined as the amount of sand transported normal to the bedform axis [5]. If the transport rates of the bimodal wind differ, then asymmetric barchans are obtained, which may have one limb extended downwind (Figs. 3f,g; see Ref. [8]). Finally, while longitudinal dunes on top of bedrock look straight (Fig. 3e and Refs. [6,8,43,45,46]), dunes on a sand bed display the characteristic meandering

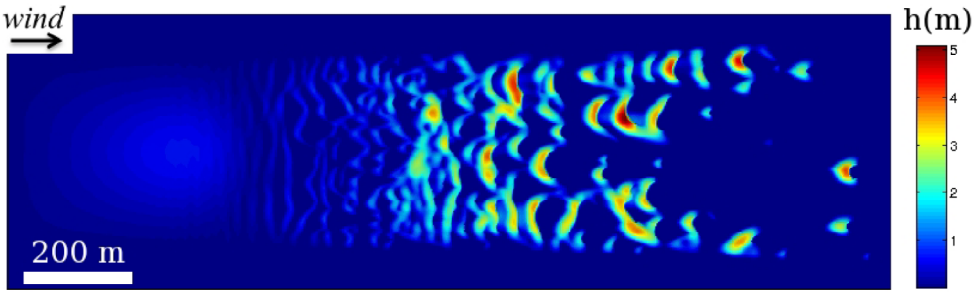

Fig. 4. Genesis of a barchan dune field from a flat sand hill under saturated flux [16].

of longitudinal seif dunes [47] (Fig. 3h), which is due to sand exchange between the seif dune and the small transverse bedforms in the interdune [6].

Dune fields – Figure 4 shows the simulation of the birth of a barchan field from a flat sand hill [16]. The surface of such a hill is unstable due to the hydrodynamic instability discussed in Section 2, and develops small transverse dunes. Their length scales with the flux saturation length L_{sat}, and, under saturated influx conditions, the hill's windward foot is not eroded out as in flume experiments of barchan belts [49]. The hill becomes a permanent sediment source for the generation of transverse dunes. Once these dunes reach the bare ground, they become unstable and give place to barchans (Fig. 4).

The complex origin of the transverse instability has been analyzed by various researchers using various approaches [33,50–54]. Crucial elements for the instability that have been identified by these studies are a limited and variable windward sand supply to the transverse dune, the (inverse) size-dependence of its speed, and the limited efficiencies of transverse sand transport mechanisms on the upwind and downwind sides of the dune. For instance, simulations using the minimal model [50] showed that any height perturbation along the transverse dune profile amplifies exponentially with growth rate determined by the dune turnover time, while the fastest growing mode nearly equals the average cross-stream width of the emerging barchans. Experiments [45] showed that an isolated transverse sand bar under unidirectional water stream and vanishing incoming sediment flux fully breaks into a chain of barchans – the reverse process of an isolated transverse barchans chain leading to a transverse dune does not occur. Field studies [55] reported a similar type of transverse instability of aeolian megaripples, which are intermediate to ripples and dunes. However, the growth of the transverse instability may be suppressed if the dunes are closely spaced, on a sand bed, or subject to reversing winds, which remains to be investigated in the future [33,56]. Small dunes may be produced from the sand of barchans participating in collisions, thereby avoiding the formation of one single dune from dune merging and providing a mechanism of dune size regulation [57–59]. Whether collisions or surface-wave instabilities induced by changes in wind direction [60] provide the most relevant size regulation mechanism in barchan fields is currently a matter of strong debate [61–64].

Dune mobility against vegetation – Reference [65] extended the model to incorporate the growth of a vegetation cover on the sand terrain and its effect on sand transport [65]. The simulations indicate that the relevant parameter for the dune shape is the fixation index $\theta = Q_0/(V^{1/3}V_v)$, where Q_0 is the bulk sand flux and V is the dune volume. This fixation index gives the ratio between erosion rate, which is proportional to $Q_0/V^{1/3}$, and the vegetation growth rate, V_v. Barchans are obtained if $\theta \gtrsim 0.5$, while for smaller θ the barchan inverts its shape leading to an U-shaped parabolic dune. Field observations support this prediction [66].

Quantitative agreement was found between the shape of simulated vegetated dunes and their real counterparts [67–69].

Dune fields with an exposed water table – Reference [70] presented an extended version of the model that includes the effect of seasonal inundation of interdune areas [71–73]. In the model, the shear stress is computed for the whole envelope comprising the dune surface and the water level, while underwater flux can occur only through avalanches [70]. Simulations using such a model reproduce the sinusoisodal shape of barchanoidal dunes separated by water ponds when the period of rise and sink of the water table is comparable to the dune turnover time [70]. The results suggest that an exposed water table can attenuate the growth of the transverse dune instability.

3 Open tasks

As summarized in the foregoing overview, a strongly coarse-grained mean-field representation of the complex process of aeolian sand transport has been remarkably successful as a starting point for the morphodynamic modeling of a wide variety of aeolian structures. These successes notwithstanding, there remain some conceptual and practical limitations of the present modeling approaches. In the following, we summarize some ongoing work aimed at overcoming these limitations, which partly lie in the morphodynamic framework and partly in the sand-transport model itself.

3.1 Open problems of the sediment transport model

The modeling of the formation and migration of sand dunes and whole assemblies of dunes requires a sand transport model that is both physically correct and numerically efficient. The mean-field model that was briefly reviewed above [12] and employed in many previous analytical and numerical studies, was tailored to provide a physically reasonable representation of the overall sand flux as a function of the wind strength on complex topographies, at low numerical cost. There are clearly many ways to venture beyond such a model, ranging from purely analytical approaches [74,75] over hybrids combining analytical and numerical elements [76–79] to expensive grain-scale numerical simulations [80,81]. An increasing amount of numerical elements generally allows for the inclusion of increasing amounts of details. But this usually comes at a loss of numerical efficiency. Moreover, at the present stage, even grain-scale numerical simulations cannot avoid fairly drastic idealizations.

There are three main reasons for the recent interest in refined models of aeolian sand transport: a surge in new grain-scale experiments that produced a wealth of quantitative laboratory and wind-tunnel data characterizing the grain-bed interactions (rebound, splash) and the saltation process in general [82–90], the wish to increase the accuracy of the sand flux equations employed in morphodynamic modeling, and finally the need, arising in applications, to account for mesoscale details that are wiped out in the derivation of any mean-field model. Important examples for such applications thought to be sensitive to finer details are ripple formation, dust emission, and plant invasion. Mean-field models that map all grain trajectories onto a single representative trajectory are naturally blind to such important phenomena. They simply do not resolve the broad distribution of grain trajectories and velocities, traditionally classified in terms of the transport modes of suspension, saltation, and creep/reptation or bedload, and their dependence on the grain size, the wind strength, and further ambient parameters.

Compared to full-fledged grain-scale simulations and hybrid numerical approaches, the analytical models that were recently developed to address the mesoscale structure are much simpler, numerically more efficient, and more easily implemented in

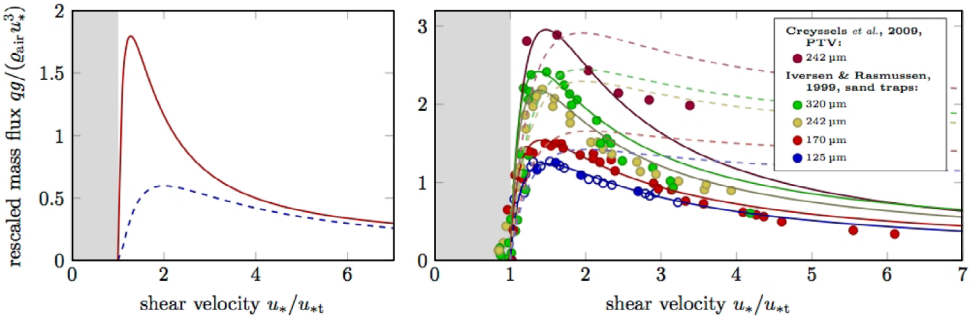

Fig. 5. Predictions for the aeolian sand flux by the two-species continuum model (after Ref. [75]). The panels depict reduced stationary sand transport rates as a function of the wind strength, quantified by the shear velocity u_*, where an overall factor proportional to u_*^3 is divided out. *Left panel:* flux balance between the two idealized grain species of "reptons" (dashed) and "saltons" (solid). *Right panel:* overall flux predicted by the two-species continuum model [75] (solid lines) and by the Sauermann model [12] (dashed lines) compared to wind tunnel data from Refs. [88,91], for various grain diameters, as indicated.

morphodynamic models. Their description of the saltation process is more sophisticated, yet not substantially more complex than in the Sauermann model [12], and they are numerically equally efficient. They implement a comparable amount of additional grain-scale information, but take slightly different routes. The model of Ref. [74] considers the grain-scale kinematics and the momentum and energy balance of the grain-bed interactions more closely. At the core of the two-species model of Ref. [75] lies a parametrization of the mobilized grain population by two effective subpopulations, roughly corresponding to the intuitive categories of saltation and bedload, and their mutual balance (Fig. 5). Both models yield quantitatively improved predictions for the sand flux compared to the Sauermann model [12]. For the two-species model [75], moreover, a comprehensive test of its mesoscale predictions against a large variety of experimental data recently became available [32]. Altogether, the success of these refined models suggests that a faithful description of various processes sensitive to the mesostructure of aeolian transport might in the future be achieved with analytical models, without excessive recourse to the laborious grain-scale simulations and hybrid approaches.

3.2 Open problems of the morphodynamic model

In addition to the open problems of the continuum sediment transport model discussed above, there are future plans of improvements and applications of the morphodynamic model (discussed below).

3.2.1 Secondary flow effects and the separation bubble model

Sand transportation and deposition on the dune surface can be affected by two types of secondary flow. The first type is characterized by the reversed circular motion in the separation bubble (Fig. 2b), which occurs when the wind encounters the dunes body *perpendicularly*. Since net downwind transport in the bubble essentially vanishes, the shear stress there is simply set to zero in the model [13]. However, the reversed flow can enhance deposition on the dune lee side and contribute to shaping the slip face [92]. Neglecting this secondary flow may lead to incorrect numerical prediction of the

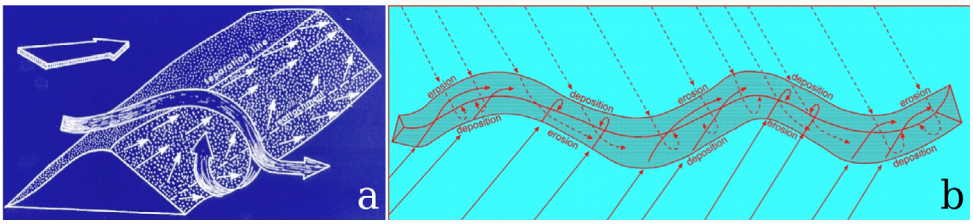

Fig. 6. (a) 3-D sketch showing the separation of flow at the lee side of a linear (seif) dune and the diverted flow. After Ref. [99]. (b) Schematic diagram showing the dynamic processes acting on a winding linear (seif) dune that is under bimodal wind regime with $\theta_w = 110^\circ$. One wind direction is given by hatched lines and the other by continuous lines. After Ref. [3].

profile of interdune areas in a field of closely-spaced dunes [72,93]. CFD simulations of the turbulent wind flow over transverse dunes revealed a linear scaling between the surface wind shear velocity (which is proportional to the average flow velocity gradient in the turbulent boundary layer flow [37]) associated with the reversed flow at the lee and the upwind shear velocity [94]. It was shown that the size of the zone of recirculating flow depends on the dune crest-brink distance, the upwind shear velocity and the interdune spacing [94–98]. The separation bubble of the morphodynamic model should be improved to account for these insights.

The second type of secondary flow occurs when the wind encounters a dune body *obliquely*. In this case, the secondary reversed circular motion in the lee side continues to flow along the lee slope [47,100] (Fig. 6a). This type of secondary flow causes transport along the crest-line of an elongating longitudinal seif dune under a bimodal wind. Zones of erosion and deposition on both flanks of the meandering dune alternate as each wind direction encounters the dune crest-line obliquely or perpendicularly (see Fig. 6b). Extension of the model to include both types of secondary flow is thus required in order to improve the quantitative assessment of seif dunes [6]. Secondary flow effects should contribute to the growth and shape of accumulating star dunes under multidirectional winds, in particular for the elongation of the dune arms [9], which remains to be confirmed through numerical simulations [10].

3.2.2 Sand induration and biogenic crust

In order to make realistic simulations of dune fields, the effect of a stabilizing agent that is present in *all* cold and arid regions of the Earth must be incorporated in the model. In the absence of a dense distribution of higher plants (macrophytes), much of the semi-arid and arid surfaces are covered by *microphytic* communities of small non-vascular plants [101,102]. These microphytic communities, containing various combinations of lichen, mosses, algae, fungi, bacteria and cyanobaceria, form the so-called *biogenic crusts* within and over a wide range of rock and soil substrates [103]. While it has been shown that biogenic crusts can lead to sand induration and cause significant attenuation of rates of sediment transport [104–106], their role for morphological changes on dune surface is still uncertain [107,108]. Indeed, very little modeling effort has been made so far to understand dune dynamics with biogenic crust. An exception is Ref. [109], in which a mean field model was proposed to estimate the mean coverage of bare sand, vegetation and biogenic crust due to average rainfall and wind power in a dune field. The model of Ref. [109] predicts that under very low precipitation (between 20 and 50 mm/yr on annual average) and no winds (DP=0) a dune can be fully stabilized by crust without vegetation. However, all crusted dunes (in Australia, Kalahari and the Negev) are covered sparsely by vegetation.

Biogenic crust will not spread on sand dunes surfaces as long as the sand is easily transported by the wind.

Sand induration by ice or mineral salts, which act as intergranular cement, could explain the formation of straight linear dunes ("lee dunes") in the north polar region of Mars known as "Chasma Boreale" [110]. Such straight dunes occur side-by-side with barchans, which indicate unidirectional winds [110]. According to the conceptual model of Ref. [3], sand encountering an indurated barchan from the upwind direction will be accumulated in the dune wake giving rise to a dome-like dune [110,111]. The short lee dune that emerges in the barchan wake then stabilizes in time but continues lengthening parallel to the wind, giving rise to a straight, sharp-crested lee dune. Such an origin of Martian lee dunes remains to be verified in numerical simulations [94,110].

3.2.3 Dune response to climatic changes

Although the factors governing dune morphology have been studied since almost a century, the need for understanding dune response to climatic changes has become more apparent in the last few decades owing to increased concern about the human and environmental consequences of desertification [112,113].

One intriguing phenomenon is that, in some dune fields, bare mobile dunes may coexist with vegetated stabilized dunes. Refs. [114,115] introduced a mean field model for the average dune vegetation cover in a dune field driven by wind power and rainfall, which explains the bi-stability of active and fixed dunes under the same climate conditions. A vegetated dune can become active when the wind power is sufficiently high to cause the decay of vegetation, or after a long drought that brought the average annual rainfall to values smaller than 60 mm. Once the dune is active, it can be stabilized if the wind power decreases to a much lower value, such that vegetation growth cannot be suppressed (see Fig. 6 of Ref. [115]). This hysteresis model was used to predict the future activity of the stabilized Kalahari and the Australian Deserts, based on two global circulation models [116]. The results show that these two large deserts are not going to reactivate towards the end of the 21st century. An extended version of this model, which included the effect of grazing on the vegetation cover and the growth of biogenic crust [109], revealed bistability of crust and vegetated stabilized dunes for low precipitation and wind power. Different examples of stabilized dune fields support the model predictions [109].

References [114–116] provided thus insights on the effect of climatic changes and human activities on vegetation and biogenic crust cover, which should be incorporated into the morphodynamic dune model. The future application of this model has the potential to improve our quantitative understanding of the fixation, remobilization, growth and elongation dynamics of different dune types in response to droughts, changes in wind regime, availability of mobile sediment, vegetation or biogenic crust cover.

3.2.4 Modeling aeolian landscapes in presence of anti-desertification measures

Sand stabilization is a fundamental aspect of conservation and anti-desertification activities [92]. Different anti-desertification measures involve the use of artificial windbreaks like fences (Fig. 7a) for reducing wind velocity, blocking saltating sand or protecting crops or loose soil from erosion. Wind tunnel studies [117–120] and numerical simulations [121–124] shed light on the characteristics of the turbulent wind flow and sand flux around different types of fences. Still, the dynamics of dune formation around windbreaks is quantitatively poorly understood [125,126].

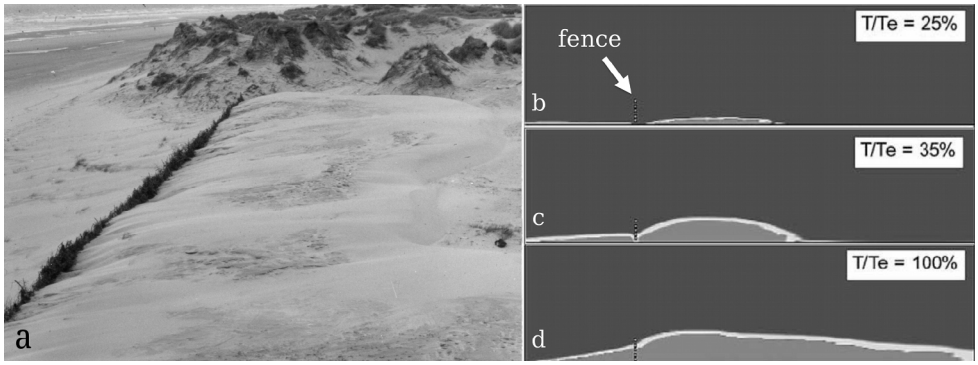

Fig. 7. (a) Accretion of wind-blown sand behind a brushwood fence, Formby, Merseyside, UK (image credit: Kenneth Pye); (b–d) modeling snow dune formation around a vertically erected fence using a CFD two-phase flow model [127]. The figures show snapshots of the deposition stages using a 50% porous fence at different time steps T/T_e, where T_e is number of time steps needed for the surface to reach equilibrium. Adapted from Ref. [127].

Reference [127] introduced a CFD two-phase flow model for simulating the transport of wind-blown particles of different materials (including sand and snow) through a porous fence and the concatenated formation of a dune (Figs. 7b–d). However, such a model is one-way coupled, that is it neglects the momentum loss of the air due to acceleration of the particles. Therefore, this model lacks a physical description of the sediment flux saturation length, which leads to the emergence of a minimal dune size (Fig. 2a). It would be interesting to develop a numerical tool which couples the continuum model for sediment transport of Refs. [12–14] with the CFD calculations of the average shear stress over the envelope comprising fences and sand surface [127,128]. Numerical simulations using such a tool could elucidate the long-term dynamics of the sand topography in presence of different anti-desertification measures, including the use of arrays of fences of different spacing and porosities and the cultivation of natural stabilizing agents like vegetation and biogenic crusts [129].

4 Concluding remarks

The list of ongoing work and future plans presented here is by no means exhaustive. For instance, important open questions regarding extraterrestrial dunes [37,44], such as the origins of Venusian transverse dunes and of Titan's linear dunes, remain to be addressed. However, the continuum sand transport model must be first extended to calculate dune formation in the subaqueous regime. Finally, numerical simulations using the model could assist or partially replace expensive, large-scale experiments such as the ones of Ref. [7] to elucidate the formative stages of dune fields under complex wind regimes.

Hans Herrmann is gratefully acknowledged for suggestions and inspiring discussions. We thank Kenneth Pye for providing us with Fig. 7a and Marc Lämmel for a critical reading of the manuscript and help with Fig. 5. We also acknowledge the German Science Foundation (DFG) for funding through the Cluster of Excellence "Engineering of Advanced Materials" and the Collaborative Research Center SFB814 (Additive Manufacturing). K.K. and H.T. were supported by the National Science Foundation under Grant No. NSFPHY11-25915 to the Kavli Institute of Theoretical Physics and by the German Israeli Foundation for Scientific Research and Development (GIF) under Grant No. 4411-1.02/8.44. J.S.A. thanks

CNPq, CAPES and FUNCAP for financial support. The authors gratefully acknowledge the computing time granted by the John von Neumann Institute for Computing (NIC) and provided on the supercomputer JUROPA at Jülich Supercomputing Centre (JSC).

References

1. R.A. Bagnold, *The Physics of Blown Sand and Desert Dunes* (Methuen, London, 1941)
2. S. Fryberger, G. Dean, *A Study of Global Sand Seas* (U.S. Geological Survey, Reston, VA, 1979), p. 137, prof. Pap., 1052
3. H. Tsoar, Lect. Notes Phys. **582**, 403 (2001)
4. H. Tsoar, Physica A **357**, 50 (2005)
5. D.M. Rubin, R.E. Hunter, Science **237**, 276 (1987)
6. E.J.R. Parteli, O. Durán, H. Tsoar, V. Schwämmle, H.J. Herrmann, Proc. Natl. Acad. Sci. **106**, 22085 (2009)
7. L. Ping, C. Narteau, Z. Dong, Z. Zhang, S. Courrech du Pont, Nat. Geosci. **7**, 99 (2014)
8. E.J.R. Parteli, O. Durán, M.C. Bourke, H. Tsoar, T. Pöschel, H.J. Herrmann, Aeolian Res. **12**, 121 (2014)
9. N. Lancaster, Sedimentology **36**, 273 (1989)
10. D. Zhang, C. Narteau, O. Rozier, S. Courrech Du Pont, Nat. Geosci. **5**, 463 (2012)
11. B. Andreotti, A. Fourrière, F. Ould-Kaddour, B. Murray, P. Claudin, Nature **457**, 1120 (2009)
12. G. Sauermann, K. Kroy, H.J. Herrmann, Phys. Rev. E **64**, 31305 (2001)
13. K. Kroy, G. Sauermann, H.J. Herrmann, Phys. Rev. Lett. **88**, 054301 (2002)
14. K. Kroy, G. Sauermann, H.J. Herrmann, Phys. Rev. E **66**, 031302 (2002)
15. V. Schwämmle, H.J. Herrmann, Eur. Phys. J. E **16**, 57 (2005)
16. O. Durán, E.J.R. Parteli, H.J. Herrmann, Earth Surf. Proc. Landforms **35**, 1591 (2010)
17. P.S. Jackson, J.C.R. Hunt, Q. J. R. Meterol. Soc. **101**, 929 (1975)
18. W.S. Weng, J.C.R. Hunt, D.J. Carruthers, A. Warren, G.F.S. Wiggs, I. Livingstone, I. Castro, Acta Mech. (Suppl.) **2**, 1 (2010)
19. O. Zeman, N.O. Jensen, Risø National Laboratory **M-2738** (1988)
20. J.H. van Boxel, S.M. Arens, P.M. van Dijk, Earth Surf. Proc. Landforms **24**, 255 (1999)
21. B. Andreotti, P. Claudin, S. Douady, Eur. Phys. J. B **28**, 341 (2002)
22. B. Andreotti, P. Claudin, O. Pouliquen, Geomorphology **123**, 343 (2010)
23. S. Fischer, M.E. Cates, K. Kroy, Phys. Rev. E **77**, 031302 (2008)
24. G. Sauermann, P. Rognon, A. Poliakov, H.J. Herrmann, Geomorphology **36**, 47 (2000)
25. K. Kroy, X. Guo, Phys. Rev. Lett. **93**, 039401 (2004)
26. J.D. Pelletier, J. Geophys. Res. **118**, 2406 (2013)
27. P. Hersen, S. Douady, B. Andreotti, Phys. Res. Lett. **89**, 264301 (2002)
28. C. Groh, A. Wierschem, N. Aksel, I. Rehberg, C.A. Kruelle, Phys. Rev. E **78**, 021304 (2008)
29. C. Groh, I. Rehberg, C.A. Kruelle, New J. Phys. **11**, 023014 (2009)
30. K. Kroy, S. Fischer, B. Obermayer, J. Phys.: Condens. Matter **17**, S1229 (2005)
31. E.J.R. Parteli, O. Durán, H.J. Herrmann, Phys. Rev. E **75**, 011301 (2007)
32. M. Lämmel, A. Meiwald, K. Kroy [`arXiv:1405.0624v1`] (2014)
33. L. Guignier, H. Niiya, H. Nishimori, D. Lague, A. Valance, Phys. Rev. E **87**, 052206 (2013)
34. B.T. Werner, Geology **23**, 1107 (1995)
35. A.R. Lima, G. Sauermann, H.J. Herrmann, K. Kroy, Physica A **310**, 487 (202)
36. E.J.R. Parteli, H.J. Herrmann, Physica A **327**, 554 (2003)
37. J.F. Kok, E.J.R. Parteli, T.I. Michaels, D. Bou Karam, Rep. Prog. Phys. **75**, 106901 (2012)
38. A.C.W. Baas, in *Treatise on Geomorphology*, edited by J. Shroder, N. Lancaster, D.J. Sherman, A.C.W. Baas, Vol. 11 (Academic Press, San Diego, CA, 2013), p. 313
39. A. Fourrière, P. Claudin, B. Andreotti, J. Fluid Mech. **649**, 287 (2010)
40. F. Charru, B. Andreotti, P. Claudin, Annu. Rev. Fluid Mech. **45**, 469 (2013)

41. T. Pähtz, J.F. Kok, E.J.R. Parteli, H.J. Herrmann, Phys. Rev. Lett. **111**, 218002 (2013)
42. G. Sauermann, J.S. Andrade Jr., L.P. Maia, U.M.S. Costa, A.D. Araújo, H.J. Herrmann, Geomorphology **54**, 245 (2003)
43. E.J.R. Parteli, H.J. Herrmann, Phys. Rev. Lett. **98**, 198001 (2007)
44. M.C. Bourke, N. Lancaster, L.K. Fenton, E.J.R. Parteli, J.R. Zimbelman, J. Radebaugh, Geomorphology **121**, 1 (2010)
45. E. Reffet, S. Courrech du Pont, P. Hersen, S. Douady, Geology **38**, 491 (2010)
46. K. Taniguchi, N. Endo, H. Sekiguchi, Geomorphology **179**, 286 (2012)
47. H. Tsoar, Sedimentology **30**, 567 (1983)
48. O. Durán, H.J. Herrmann, J. Stat. Mech. **P07011**, 1591 (2006)
49. A. Katsuki, M. Kikuchi, N. Endo, J. Phys. Soc. Jpn. **74**, 878 (2005)
50. E.J.R. Parteli, J.S. Andrade Jr., H.J. Herrmann, Phys. Rev. Lett. **107**, 188001 (2011)
51. H.P.M. Melo, E.J.R. Parteli, J.S. Andrade Jr., H.J. Herrmann, Physica A **391**, 4606 (2012)
52. L. Guignier, A. Valance, D. Lague (2012), `http://hal.archives-ouvertes.fr/hal-00933534/`
53. H. Niiya, A. Awazu, H. Nishimori, Phys. Rev. Lett. **108**, 158001 (2012)
54. H. Niiya, A. Awazu, H. Nishimori, Aeolian Res. **9**, 63 (2013)
55. H. Yizhaq, I. Katra, J.F. Kok, O. Isenberg, Geology **40**, 459 (2012)
56. D.M. Rubin, Earth-Sci. Rev. **113**, 176 (2012)
57. V. Schwämmle, H.J. Herrmann, Nature **426**, 619 (2003)
58. O. Durán, V. Schwämmle, H.J. Herrmann, Phys. Rev. E **72**, 021308 (2005)
59. O. Durán, V. Schwämmle, P.G. Lind, H.J. Herrmann, Granul. Matter **11**, 7 (2009)
60. H. Elbelrhiti, P. Claudin, B. Andreotti, Nature **437**, 720 (2005)
61. H. Elbelrhiti, B. Andreotti, P. Claudin, J. Geophys. Res. **113**, F02S15 (2008)
62. O. Durán, V. Schwämmle, P.G. Lind, H.J. Herrmann, Nonlinear Process. Geophys. **18**, 455 (2011)
63. M. Génois, S.C. Du Pont, P. Hersen, G. Grégoire, Geophys. Res. Lett. **40**, 3909 (2013)
64. S.L. Worman, A.B. Murray, R. Littlewood, B. Andreotti, P. Claudin, Geology **41**, 1059 (2013)
65. O. Durán, H.J. Herrmann, Phys. Rev. Lett. **97**, 188001 (2006)
66. M.D. Reitz, D.J. Jerolmack, R.C. Ewing, R.L. Martin, Geophys. Res. Lett. **37**, L19402 (2010)
67. O. Durán, M.V.N. Silva, L.J.C. Bezerra, H.J. Herrmann, L.P. Maia, Geomorphology **102**, 460 (2008)
68. M.C.M.M. Luna, E.J.R. Parteli, O. Durán, H.J. Herrmann, Geomorphology **129**, 215 (2011)
69. O. Durán, L. Moore, Proc. Natl. Acad. Sci. **110**, 17217 (2013)
70. M.C.M.M. Luna, E.J.R. Parteli, H.J. Herrmann, Geomorphology **159-160**, 169 (2012)
71. G. Kocurek, M. Townsley, E. Yeh, K. Havholm, M.L. Sweet, J. Sediment. Petrol. **62**, 622 (1992)
72. E.J.R. Parteli, V. Schwämmle, H.J. Herrmann, L.H.U. Monteiro, L.P. Maia, Geomorphology **81**, 29 (2006)
73. H. Tsoar, N. Levin, N. Porat, L.P. Maia, H.J. Herrmann, S.H. Tatumi, V. Claudino-Sales, Quat. Res. **71**, 217 (2009)
74. T. Pähtz, J.F. Kok, H.J. Herrmann, New J. Phys. **14**, 043035 (2012)
75. M. Lämmel, D. Rings, K. Kroy, New J. Phys. **14**, 093037 (2012)
76. B. Andreotti, J. Fluid Mech. **510**, 47 (2004)
77. M.P. Almeida, J.S. Andrade Jr., H.J. Herrmann, Phys. Rev. Lett. **96**, 018001 (2006)
78. M.P. Almeida, E.J.R. Parteli, J.S. Andrade Jr., H.J. Herrmann, Proc. Natl. Acad. Sci. **105**, 6222 (2008)
79. J.F. Kok, N.O. Renno, J. Geophys. Res. **114**, D17204 (2009)
80. O. Durán, B. Andreotti, P. Claudin, Phys. Fluids **24**, 103306 (2012)
81. M.V. Carneiro, N.A.M. Araújo, T. Pähtz, H.J. Herrmann, Phys. Rev. Lett. **111**, 058001 (2013)

82. S.L. Namikas, Sedimentology **50**, 303 (2003)
83. X. Liu, Z. Dong, Geomorphology **60**, 371 (2004)
84. D. Beladjine, M. Ammi, L. Oger, A. Valance, Phys. Rev. E **75**, 061305 (2007)
85. K.R. Rasmussen, M. Sørensen, J. Geophys. Res. **113**, F02S12 (2008)
86. M. Ammi, L. Oger, D. Beladjine, A. Valance, Phys. Rev. E **79**, 021305 (2009)
87. A. Valance, J. Crassous, Eur. Phys. J. E **30**, 43 (2009)
88. M. Creyssels, P. Dupont, A.O. El Moctar, A. Valance, I. Cantat, J.T. Jenkins, J.M. Pasini, K.R. Rasmussen, J. Fluid Mech. **625**, 47 (2009)
89. L. Kang, X. Zou, Geomorphology **125**, 361 (2011)
90. T.D. Ho, A. Valance, P. Dupont, A. El Moctar, Phys. Rev. Lett. **85**, 052301 (2011)
91. J.D. Iversen, K.R. Rasmussen, Sedimentology **46**, 723 (1999)
92. K. Pye, H. Tsoar, *Aeolian Sand and Sand Dunes* (Uwin Hyman, London, 1990)
93. V. Schwämmle, H.J. Herrmann, Earth Surf. Proc. Landforms **29**, 769 (2004)
94. A.D. Araújo, E.J.R. Parteli, T. Pöschel, J.S. Andrade Jr., H.J. Herrmann, Sci. Rep. **3**, 2858 (2013)
95. D.R. Parsons, G.F.S. Wiggs, I.J. Walker, R.I. Ferguson, B.G. Garvey, Environ. Model. Softw. **19**, 153 (2004)
96. H.J. Herrmann, J.S. Andrade Jr., V. Schatz, G. Sauermann, E.J.R. Parteli, Physica A **357**, 44 (2005)
97. V. Schatz, H.J. Herrmann, Geomorphology **81**, 207 (2006)
98. A.D. Ferreira, S.R. Pinheiro, S.C. Francisco, Environ. Fluid Mech. **13**, 557 (2013)
99. H. Tsoar, Geographys. **76**, 144 (1990)
100. H. Tsoar, D.H. Yaalon, Sediment. Geol. **36**, 25 (1983)
101. O.L. Lange, DFG Forschung Magazin **4**, 14 (2003)
102. J. Belnap, Science **340**, 1533 (2013)
103. A. Karnieli, H. Tsoar, Int. J. Remote Sensing **16**, 369 (1995)
104. J.D. Williams, J.P. Dobrowolski, N.E. West, D.A. Gillette, Trans. ASAE **38**, 131 (1995)
105. B. Marticorena, G. Bergametti, D. Gillette, J. Belnap, J. Geophys. Res. **102**, 23277 (1997)
106. J. Belnap, D.A. Gillette, J. Arid Environ. **39**, 133 (1998)
107. T. Fischer, A. Yair, M. Veste, Biogeosci. Discuss. **9**, 12711 (2012)
108. R. Amir, S. Kinast, H. Tsoar, H. Yizhaq, E. Zaady, Y. Ashkenazy, J. Geophys. Res. **119**, 437 (2014)
109. S. Kinast, E. Meron, H. Yizhaq, Y. Ashkenazy, Phys. Rev. E **87**, 020701(R) (2013)
110. V. Schatz, H. Tsoar, K. Edgett, E.J.R. Parteli, H.J. Herrmann, J. Geophys. Res. **111**, E04006 (2006)
111. R.C. Kerr, J.O. Nigra, Am. Assoc. Pet. Geol. Bull. **36**, 1541 (1952)
112. D.S.G. Thomas, M. Knight, G.F.S. Wiggs, Nature **435**, 1218 (2005)
113. H. Tsoar, in *Treatise on Geomorphology*, edited by J. Shroder, N. Lancaster, D.J. Sherman, A.C.W. Baas, Vol. 11 (Academic Press, San Diego, CA, 2013), p. 414
114. H. Yizhaq, Y. Ashkenazy, H. Tsoar, Phys. Rev. Lett. **98**, 188001 (2007)
115. H. Yizhaq, Y. Ashkenazy, H. Tsoar, J. Geophys. Res. **114**, F01023 (2009)
116. Y. Ashkenazy, H. Yizhaq, H. Tsoar, Clim. Change **112**, 901 (2012)
117. R. Baltaxe, Arch. Meteorol. Geophys. Bioklimatol. Ser. B **15**, 3 (1967)
118. J.D. Wilson, Boundary-Lay. Meteorol. **38**, 37 (1987)
119. S.J. Lee, H.B. Kim, J. Wind Eng. Ind. Aerod. **80**, 311 (1999)
120. T. Tsukahara, Y. Sakamoto, D. Aoshima, M. Yamamoto, Y. Kawaguchi, Exp. Fluids **52**, 877 (2012)
121. K. Hatanaka, S. Hotta, Int. J. Numer. Meth. Fl. **24**, 1291 (1997)
122. J.D. Wilson, J. Appl. Meteorol. **43**, 1392 (2004)
123. J.L. Santiago, F. Martín, A. Cuerva, N. Bezdenejnykh, A. Sanz-Andrés, Atmos. Environ. **41**, 6406 (2007)
124. J.P. Bitog, I.B. Lee, M.H. Shin, S.W. Hong, H.S. Hwang, I.H. Seo, J.I. Yoo, K.S. Kwon, Y.H. Kim, J.W. Han, Atmos. Environ. **43**, 4612 (2009)

125. R.P. Savage, *Coastal Engineering 1962, Proceedings of the 8th International Conference, Mexico City, Mexico* (American Society of Civil Engineers, 1963), p. 380
126. K.F. Nordstrom, N.L. Jackson, A.L. Freestone, K.H. Korotky, J.A. Puleo, Geomorphology **179**, 106 (2012)
127. S. Alhajraf, Environ. Model. Softw. **19**, 163 (2004)
128. A.D. Araújo, J.S. Andrade Jr., L.P. Maia, H.J. Herrmann, Granul. Matter **11**, 193 (2009)
129. M. Veste, S.W. Breckle, S.W. Eggert, T. Littmann, Basic Appl. Dryland Res. **5**, 1 (2011)